# REFERENCES


[1] Pan, L. S., and Kania, D. R. *Diamond : Electric properties and applications.* USA: Kluwer Academic Publishers, 1995.

[2] May, P. W. Diamond thin films: a 21-st century material. *PHILOSOPHICAL TRANSACTIONS OF THE ROYAL SOCIETY A* **358** (2000): 473-495.

[3] Spear, K. E., and Dismukes, J. P. *Synthetic diamond: Emerging CVD science and technology.* New Jersey: John Wiley & Sons, Inc, 1994.

[4] Yang, Q., Chen, W., Xiao, C., Hirose, A., and Bradley, M. Low temperature systhesis of diamond thin films through graphite etching in a microwave hygrogen plasma. *Letters to the Editor/Carbon* **43** (2005): 2618-2641.

[5] Das, D. and et al. Low surface temperature synthesis and characterization of diamond thin films. *Diamond and Related Materials* **15** (2006): 1336-1349.

[6] Chen, W and et al. Effects of gas flow rate on diamond deposition in a microwave plasma reactor. *Thin Solid Films.* **515** (2006): 1970-1975.

[7] Tachibana, T., et al. Diamond films grown by a 60-kW microwave plasma chemical vapor deposition system. *Diamond and Related Materials* **10** (2001): 1569-1572.

[8] Slabaugh, W. H., and Parsons, T. D. *General Chemistry.* $2^{nd}$ ed. USA: John Wiley & Sons, 1966.

[9] Kittel, C. *Introduction to Solid State Physics.* $7^{st}$ ed. USA: John Wiley & Sons, 1996.

[10] Gicquel, A., Hassouni, K., Silva, F., and Achard, J. CVD diamond films: From growth to applications. *Current Applied Physics* **1** (2001): 479-496.

[11] Hamers, R. J., et al. Molecular and biomolecular monolayers on diamond as interface to biology. *Diamond and Related Materials* **14** (2005): 661-668.

[12] Paosawatyanyong, B. *Frequency dependent response of diamond schottky barrier diode to large and small electrical signals.* Doctoral dissertation, Department of Electrical Engineering, Michigan State University, 1998.

[13] Liu, H., and Dandy, D. S. Studies on nucleation process in diamond CVD: an overview of recent developments. *Diamond and Related Materials* **4** (1995): 1173-1188.

[14] Zhu, W., Stoner, B. R., Williams, B. E., and Glass, J. T. Growth and Characterization of Diamond Films on Nondiamond Substrates for Electricnic Applications. *Proceeding of Institute of Electrical and Electronics Engineers* **79** (1991): 621-645.

[15] Ohring, M. *Materials Science of Thin Films Deposition and Structure* $2^{nd}$ ed. USA: Academic Press, 2002.

[16] Ye, H., et al. Nucleation and growth dynamics of diamond films by microwave plasma-enhanced chemical vapor deposition (MWPECVD). *Surface and Coatings Technology* **123** (2000): 129-133.

[17] Beckmann, R., Sobisch, B., and Wulisch, W. On the gas-phase mechanisms in MWCVD and HFCVD diamond deposition. *Diamond and Related Materials* 4 (1995): 256-260.

[18] Füner, M., Wild, C., and Kpidl, P. Simulation and development of optimized microwave plasma reactors for diamond deposition. *Surface and Coatings Technology* **116-119** (1999): 853-862.

[19] Borges, C. F. M., St-Onge, L., Moisan, M., and Gicquel, A. Influence of process parameters on diamond film CVD in a surface-wave driven microwave plasma reactor. *Thin Solid Films* **274** (1996): 3-17.

[20] Nagatsu, M., Miyake, M., and Maeda, J. Plasma CVD reactor with two-microwave oscillators for diamond film systhesis. *Thin Solid Films* **506-507** (2006): 617-621.

[21] Pleuler, E., Wild, C., Füner, M., and Koidl, P. The CAP-reactor, a novel microwave CVD system for diamond deposition. *Diamond and Related Materials* **11** (2002): 467-471.

[22] Findeling-Dufour, C., Vignes, A., and Gicquel, A. MWPACVD diamond homoepitaxial growth: role of the plasma and the substrate parameters. *Diamond and Related Materials* **4** (1995): 429-434.

[23] Lu, C. A., Chang, L., and Huang, B. R. Growth of diamond films with bias during microwave plasma chemical vapor deposition. *Diamond and Related Materials* **11** (2002): 523-526.

[24] García, M. M., Sánchez, O., Gómez-Aleixandre, and Albella, J. M. Bias enhanced nucleation process of polycrystalline diamond films. *Superficies y Vacío* **9** (1999): 115-118.

[25] Konuma, M. *Plasma Techniques for Film Deposition.* India: Alpha Science International Ltd, 2005.

[26] Grill, A. *Cold Plasma in Materials Fabrication From Fundamentals to Applications.* New York: The Institute of Electrical and Electronics Engineers, Inc., 1994.

[27] Ashfold, M. N. R., May, P. W., and Rego, C. A. Thin film diamond by chemical vapour deposition methods. (Unpublished Manuscript)

[28] Mallika, K., and Komanduri, R. Low pressure microwave plasma assisted chemical vapor deposition (MPCVD) of diamond coating on silicon nitride cutting tools. *Thin Solid Films* **396** (2001): 146-166.

[29] Silva, F. J. G., et al. Microwave plasma chemical vapour deposition diamond nucleation on ferrous substrates with Ti and Cr interlayers. *Diamond and Related Materials* **11** (2002): 1617-1622.

[30] Stiegler, J., Lang, T., Nygård-Ferguson, M., von Kaenel, Y., and Blank, E. Low temperature limits of diamond film growth by microwave plasma assisted CVD. *Diamond and Related Materials* **5** (1996): 226-230.

[31] Bühlmann, S., Blank, E., Haubner, R., and Lux, B. Characterization of ballas diamond depositions. *Diamond and Related Materials* **8** (1999): 194-201.

[32] Choi, J. H., Lee, S. H., Park, J. W. Effect of deposition conditions and pretreatments on the microstructure of MPECVD diamond thin films. *Materials Chemistry and Physics* **45** (1996): 176-179.

[33] Bénédic, F., et al. Investigations on nitrogen addition in the $CH_4$-$H_2$ gas mixture used for diamond deposition for a better understanding and the optimisation of the systhesis process. *Surface and Coatings Technology* **176** (2003): 37-49.

[34] Zhang, W., Xia, Y., Shi, W., Wang, L., and Fang, Z. Effect of substrate temperature on the selective deposition of diamond films. *Diamond and Related Materials* **9** (2000): 1687-1690.

[35] Silva, F., Gicquel, A., Chiron, A., and Achard, J. Low roughness diamond films produced at temperatures less than 600 $^oC$. *Diamond and Related Materials* **9** (2000): 1965-1970.

[36] Mortet, V., et al. Investigation of diamond growth at high pressure by microwave plasma chemical vapor deposition. *Diamond and Related Materials* **13** (2004): 604-609.

[37] Dandy, D. S. *Diamond thin films handbook: Chapter 4.* (Unpublished Manuscript)

[38] Li, X., Perkins, J., Collazo, R., Nemanich, R. J., and Sitar, Z. Investigation of the effect of the total pressure and methane concentration on the growth rate and quality of diamond thin films grown by MPCVD. *Diamond and Related Materials* **15** (2006): 1784-1788.

[39] Collin, R. E. *Foundations for Microwave Engineering.* $2^{nd}$ ed. Singapore: McGraw-Hill, Inc, 1992.

[40] Pozar, D. M. *Microwave Engineering.* $2^{nd}$ ed. USA: John Wiley & Sons, Inc., 1998.

[41] Španěl, P., Hall, E. F. H., Workman, C.T., and Smith, D. A directly coupled monolithic rectangular resonator forming a robust microwave plasma ion source for SIFT-MS. *Plasma Sources Science and Technology* **13** (2004): 282-284.

[42] Moon, S. Y., and Choe, W. Characteristics of an atmospheric microwave-induced plasma generated in ambient air by argon discharge excited in an open-ended dielectric discharge tube. *Physics of Plasmas* **9** (2002): 4045-4051.

[43] Al-Shamma'a, A. I., Wylie, S. R., Lucas, J., and Pau, C. F. Design and construction of a 2.45 GHz waveguide-based microwave plasma jet at atmospheric pressure for material processing. *Juurnal of Physics D: Applied Physics* **34** (2001): 2734-2741.

[44] Jamroz, P., and Zyrnicki, W. Optical emission characteristic of glow discharge in the $N_2$-$H_2$-$Sn(CH_3)_4$ and $N_2$-Ar-$Sn(CH_3)_4$ mixtures. *Surface and Coatings Technology.* **201** (2006): 1444-1453.

[45] National instrument of standard and technology, NIST atomic spectra database(2003). Available from: http://www.physics.nist.gov/cgi-bin/ASD/line1.pl[2006, June 9]

[46] Fabisiak, K., Banaszak, A., Kaczmarski, M., and Kozanecki, M. Structerization of CVD diamond films using Raman and ESR spectroscopy methods. *Optical Materials* **28** (2006): 106-110.

[47] Huang, B.R., Chia, C.T., Chang, M.C., Cheng, C.L. Bias effects on large area polycrystalline diamond films synthesized by the bias enhanced growth technique. *Diamond and Related Materials* **12** (2003): 26-32.

[48] Skoog, D. A., and Leary, J. J. *Principles of Instrumental Analysis.* $4^{th}$ ed. USA: Saunders College Plubishing, 1992.

[49] Leeds, S.M., Davis, T.J., May, P.W., Pickard, C.D.O., Ashfold, M.N.R. Use of different excitation wavelengths for the analysis of CVD diamond by laser Raman spectroscopy. *Diamond and Related Materials* **7** (1998): 233-237.

[50] Pattira H., *structural and tribological characterization og CrN thin films prepared by reactive dc magnetron sputtering technique.* Master's thesis, Graduate School, Chulalongkorn University, 2005.

[51] Haubner, R., and Lux, B. Deposition of ballas diamond and nano-crystalline diamond. *Refract Metals Hard Mater* **20** (2002): 93-100.

[52] Sun, Z., Shi, J.R., Tay, B.K., and Lau, S.P. UV Raman characteristics of nanocrystalline diamond films with different grain size. *Diamond and Related Materials* **9** (2000): 1979-1983.

[53] Wagner, J., Ramsteiner, M., Wild, Ch., and Koidl, P. Resonant Raman scattering of amorphous carbon and polycrystalline diamond films. *Physical Review B* **40** (1989): 1817-1824.

[54] Benndorf, C., Joeris, P., Kröger, R. Mass and optical spectroscopy of plasmas for diamond-synthesis. *Pure and Applied Chemistry* **66** (1994): 1195-1206.

[55] Asmussen, J., and Reinhard, D.K. *Diamond Films Handbook.* New York: Marcel Dekker, Inc, 2002.

[56] Park, Y. S., et al. Enhancement of diamond film quality by a cyclic deposition method under MPECVD. *Journal of Materials Science* **A209** (1996): 414-419.

[57] Hao, T., Zhang, H., Shi, C., and Han, G. Nano-crystalline diamond films synthesized at low temperature and low pressure by hot filament chemical vapor deposition. *Surface and Coating Technology* **201** (2006): 801-806.

[58] Potocky, S., et al. Investigation of nanocrysta lline diamond films grown on silicon and glass at substrate temperature below 400 °C. *Diamond and Related Materials* **16** (2007): 744-747.

# APPENDICES

# APPENDIX A

# VACUUM CHAMBER

## A.1 Vacuum Chamber Design

The main body of vacuum chamber is constructed from stainless steel cylinder with outer diameter of 219 mm and height of 254 mm. The vacuum chamber has six ports connected to the bottom plate, the front plate, the left plate, the right plate (ISO 63), the rear plate (ISO 63), and the top plate, as showed in Fig. A.1

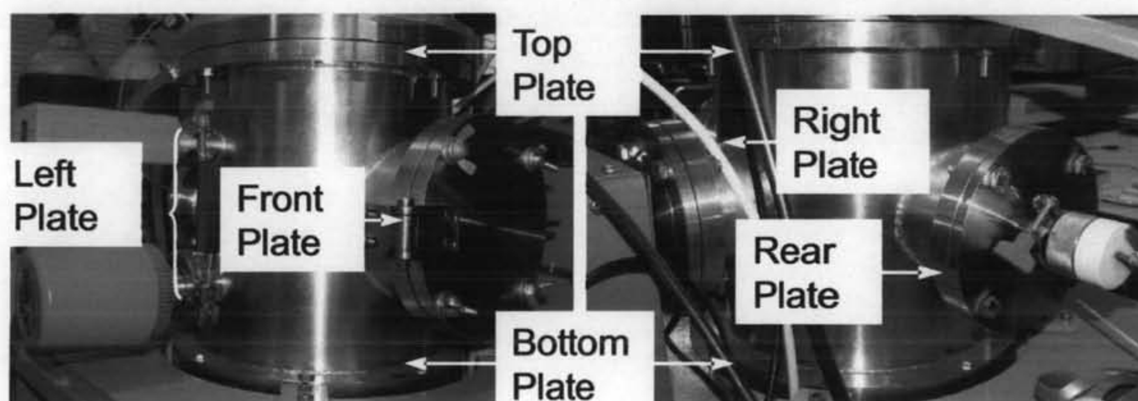


Figure A.1: The photograph of vacuum chamber.

### A.1.1 Bottom plate

The bottom plate (no.10 in Fig. A.4) is made of a 260 mm diameter stainless steel. O-ring is used as a vacuum seal for this plate. There are many equipments connected with this plate as the followings;

◇ The short flange (no.12 in Fig. A.4) which is connected with Edwards Speedivalve to allow the pressure control inside the chamber during the diamond growth processes. The Edwards ACX75 turbo molecular pump is connected with Speedivalve and backed by Edwards RV3 rotary vane pump where a base pressure of 7.0 $\times 10^{-6}$ Torr can be achieved.

◇ The short flange (no.11 in Fig. A.4) is connected with an air vent valve that allowed the chamber to be purged to the atmospheric pressure.

◇ The photograph of the punctured stainless steel substrate with diameter of 60 mm and the substrate holder are illustrated in Fig. A.2. The punctured substrate is mounted with the substrate holder, which is located axially in the vacuum chamber. The position of the punctured substrate can be adjusted and

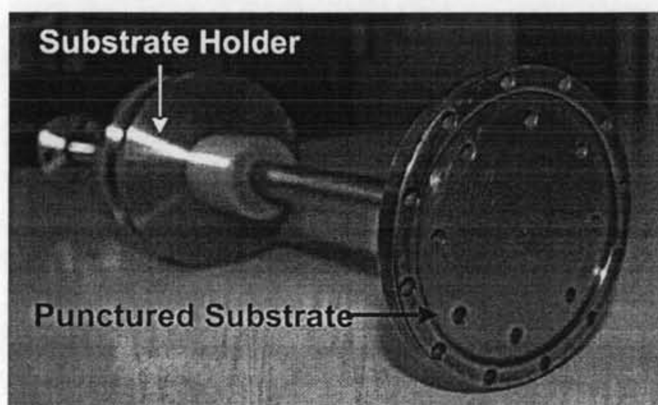


Figure A.2: The photograph of the punctured substrate and substrate holder.

acts as a short circuit part of the circular waveguide while allowed the gases to flow through. The substrate temperature was measured by a calibrated K-type thermocouple which is attached at the back of the punctured substrate, the temperature is displayed by ID-8 DIGICON temperature indicator.

◇ Port number 2 and 3 of bottom plate (Fig. C.3 in appendix C.1) are not attached with any equipment. The drawing diagram of bottom plate is showed in Fig. C.3. The photograph of bottom plate is showed in Fig. A.3.

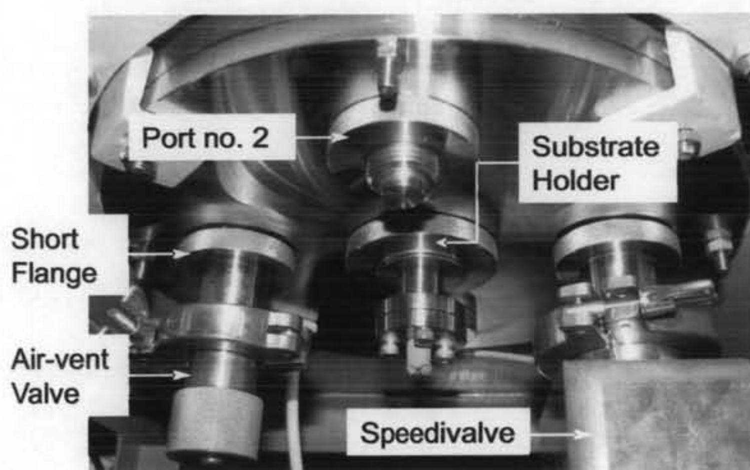


Figure A.3: The photograph of bottom plate.

### A.1.2 Front plate

The front plate (no.13 in Fig. A.4) is covered with a 154 mm diameter hinged-door and is sealed by a o-ring. This plate is used for sample loading.

### A.1.3 Left plate

Two left flanges are welded to the main body of vacuum chamber as an installation port for following equipments: (no.1, and no.2 in Fig. A.4)

◇ The short flange (NW16) which is connected with the Edwards Penning vacuum gauge used to monitor the pressure within chamber during the turbo molecular pumping process.

◇ The short flange (NW25) which is connected with the Edwards Pirani vacuum gauge used to monitor the pressure within chamber during the growth process.

### A.1.4 Right plate

The right flange (no.8 in Fig. A.4) is connected with ISO63 standard flange and is sealed by a o-ring. This flange no equipment is connected.

### A.1.5 Rear plate

The rear flange is made to comply with ISO63 standard flange size and is attached to a short flange (NW16) to be used as a feedthrough port for the K-type thermocouple.

### A.1.6 Top plate

The top plate of the chamber is connected with a donut-plate (no.3 in Fig. A.4) which is designed for water cooling and gas-inlet line. A quartz bell jar inside diameter of 76.2 mm and thickness of 6 mm is placed on this plate and a Viton o-ring is used as vacuum seal for this plate. The upper part of the donut-plate is covered by the cylindrical cavity resonator. Detail of the cavity resonator is presented in section 3.2.3. The drawing diagram of chamber components are showed in appendix C.1. The schematic diagram of MW-PECVD design is showed in Fig. A.4

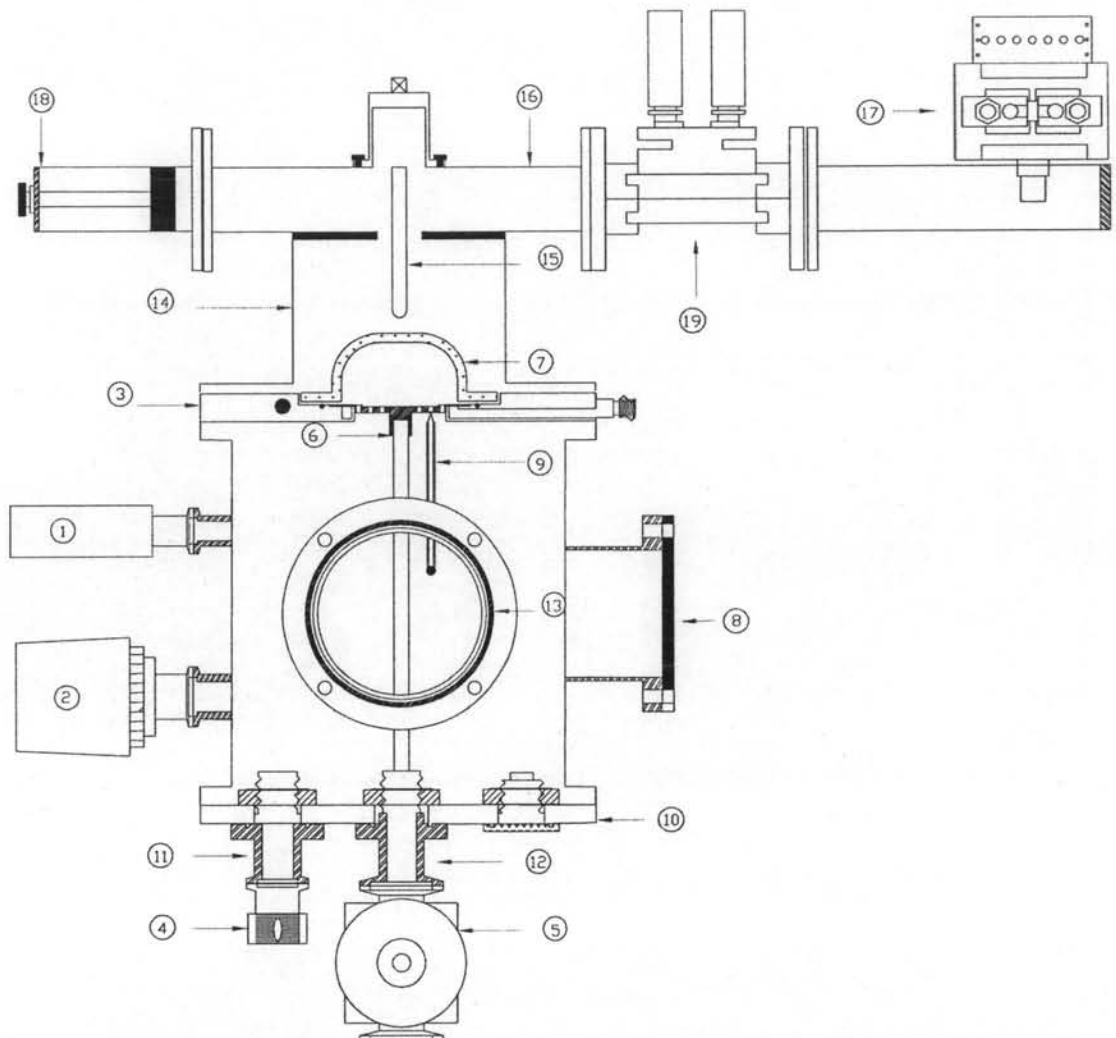

[1] Penning Gauge
[2] Pirani Gauge
[3] Donut Plate
[4] Air-Vent Valve
[5] Speedivalve
[6] Perforated Substrate
[7] Bell Jar Quartz
[8] Right Plate
[9] Type K Thermocouple
[10] Bottom Plate
[11] Short Flange NW25
[12] Short Flange NW40
[13] Loading Door
[14] Circular Cavity
[15] Brass Antenna
[16] WR-340 Waveguide
[17] Magnetron Head
[18] Short-Circuit Plunger
[19] GA3007 Dual Power Monitor

Figure A.4: The schematic diagram of MW-PECVD reactor.

# APPENDIX B

# CUTOFF FREQUENCY

## B.1 Cutoff Frequency

Both rectangular and circular waveguide are the types of transmission used lines in this study. In order to consider which electromagnetic wave can propagate, the cutoff frequency in the transmission lines must be considered. In appendix B.1, we will show the calculation details of the cutoff frequency in rectangular and circular waveguide.

### B.1.1 TE Modes in rectangular waveguide

The TE modes in an air-filled rectangular waveguide are characterized by $E_z$=0, and $H_z$ is a solution of the wave equation,

$$\nabla^2 H_z - \frac{1}{c^2}\frac{\partial^2 H_z}{\partial t^2} = 0. \tag{B.1}$$

Since $H_z(x,y,z) = H_z(x,y)e^{-i(k_g z-\omega t)}$ where $e^{-ik_g z}$ is a propagation term. Equation (B.1) can be expressed in rectangular coordinate system as

$$\frac{\partial^2 H_z}{\partial x^2} + \frac{\partial^2 H_z}{\partial y^2} + \left(\frac{\omega^2}{c^2} - k_g^2\right) H_z = 0, \tag{B.2}$$

and let

$$\frac{\omega^2}{c^2} - k_g^2 = k_c^2.$$

Also,

$$\frac{\partial^2 H_z}{\partial x^2} + \frac{\partial^2 H_z}{\partial y^2} + k_c^2 H_z = 0. \tag{B.3}$$

The partial differential of equation (B.3) can be solved by the separation variable method,

$$H_z(x,y) = \mathrm{X}(x)\,\Upsilon(y)\,, \tag{B.4}$$

and substituting into equation (B.3) to obtain

$$\frac{d^2\mathrm{X}}{\mathrm{X}dx^2} + \frac{d^2\Upsilon}{\Upsilon dy^2} + k_c^2 = 0. \tag{B.5}$$

From equation (B.5), each of terms must be equal to a constant. So

$$\frac{d^2\mathrm{X}}{dx^2} + k_x^2\mathrm{X} = 0, \tag{B.6}$$

and

$$\frac{d^2\Upsilon}{dy^2} + k_y^2\Upsilon = 0. \tag{B.7}$$

Since,

$$k_x^2 + k_y^2 - k_c^2 = 0,$$

and the general solution of equation (B.4) can be written as

$$H_z(x,y,z) = (A\cos k_x x + B\sin k_x x)\,(C\cos k_y y + D\sin k_y y)\,e^{-i(k_g z-\omega t)}. \tag{B.8}$$

The boundary conditions can be applied that

$$H_z(x,y) = 0 \qquad at\ x\ =\ 0,\ a\ \ and\ \ y\ =\ 0,\ b.$$

Therefore B and D must be equal zero and $k_x = \frac{m\pi}{a}$, $k_y = \frac{n\pi}{b}$.

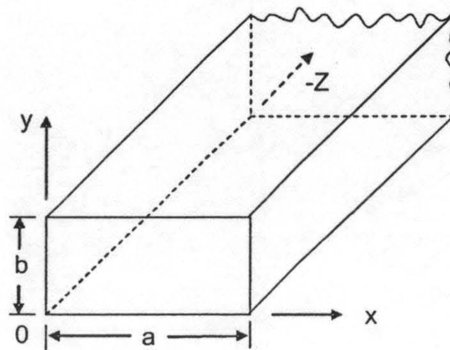


Figure B.1: Coordinates of a rectangular waveguide

Also, the propagation factor is

$$k_{g_{mn}} = \sqrt{\left(\frac{\omega}{c}\right)^2 - \left(\frac{m\pi}{a}\right)^2 + \left(\frac{n\pi}{b}\right)^2}. \quad \text{(B.9)}$$

It clearly seen that if $k_g$ is a real numbers, corresponding to a propagation mode, or

$$\left(\frac{\omega}{c}\right)^2 > k_{c_{mn}} = \sqrt{\left(\frac{m\pi}{a}\right)^2 + \left(\frac{n\pi}{b}\right)^2}. \quad \text{(B.10)}$$

Each of modes has a cutoff frequency ($f_{c_{mn}}$) given by

$$f_{c_{mn}} = \frac{c}{2\pi}\sqrt{\left(\frac{m\pi}{a}\right)^2 + \left(\frac{n\pi}{b}\right)^2}. \quad \text{(B.11)}$$

### B.1.2 TM Modes in circular waveguide

The TM modes in an air-filled circular waveguide are characterized by $H_z = 0$, and $E_z$ is a solution of the wave equation.

$$\nabla^2 E_z - \frac{1}{c^2}\frac{\partial^2 E_z}{\partial t^2} = 0. \quad \text{(B.12)}$$

Since $E_z(\rho, \phi, z) = E_z(\rho, \phi)e^{-i(k_g z - \omega t)}$ where $e^{-ik_g z}$ is a propagation term.

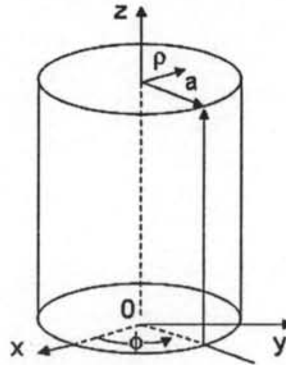


Figure B.2: Coordinates of a circular waveguide

Equation B.12 can be expressed in cylindrical coordinate system as

$$\frac{1}{\rho^2}\frac{\partial^2 E_z}{\partial \phi^2} + \frac{1}{\rho}\frac{\partial}{\partial \rho}\left(\rho\frac{\partial E_z}{\partial \rho}\right) + \left(\frac{\omega^2}{c^2} - k_g^2\right)E_z = 0, \quad \text{(B.13)}$$

and let

$$\frac{\omega^2}{c^2} - k_g^2 = k_c^2.$$

Also,

$$\frac{1}{\rho^2}\frac{\partial^2 E_z}{\partial \phi^2} + \frac{1}{\rho}\frac{\partial}{\partial \rho}\left(\rho \frac{\partial E_z}{\partial \rho}\right) + k_c^2 E_z = 0. \tag{B.14}$$

The partial differential equation of (B.14) can be solved by the separation of variables method,

$$E_z(\rho, \phi) = R(\rho)\,\Psi(\phi), \tag{B.15}$$

and substituting into equation (B.14) to obtain

$$\frac{d^2\Psi}{\Psi d\phi^2} + \frac{\rho}{R}\frac{d}{d\rho}\left(\rho\frac{dR}{d\rho}\right) + k_c^2\rho^2 = 0,$$

$$\frac{\rho^2}{R}\frac{d^2R}{d\rho^2} + \frac{\rho}{R}\left(\frac{dR}{d\rho}\right) + k_c^2\rho^2 = -\frac{d^2\Psi}{\Psi d\phi^2}. \tag{B.16}$$

From equation (B.16), each of terms must be equal to a constant, So

$$\frac{\rho^2}{R}\frac{d^2R}{d\rho^2} + \frac{\rho}{R}\left(\frac{dR}{d\rho}\right) + k_c^2\rho^2 = m^2, \tag{B.17}$$

multiply equation (B.17) by R/$\rho^2$

$$\frac{d^2R}{d\rho^2} + \frac{1}{\rho}\left(\frac{dR}{d\rho}\right) + \left(k_c^2 - \frac{m^2}{\rho^2}\right)R = 0. \tag{B.18}$$

This solution is

$$R(\rho) = AJ_m(k_c\rho) + BN_m(k_c\rho). \tag{B.19}$$

Where $J_m(k_c\rho)$ and $N_m(k_c\rho)$ are the Bessel functions of first and second kinds, respectively. Since $N_m(k_c\rho)$ is physically unacceptable for the circular waveguide problem, so B= 0. The right hand of equation (B.16), solution is

$$\Psi(\phi) = Ce^{im\phi} \qquad m = 0, 1, 2, 3... \;. \tag{B.20}$$

The solution of $E_z$ can be written as

$$E_z(\rho, \phi, z) = De^{im\phi}J_m(k_c\rho)\,e^{-i(k_g z - \omega t)}. \tag{B.21}$$

The boundary condition can be applied as

$$E_z(\rho, \phi) = 0 \qquad at\;\; \rho = a. \tag{B.22}$$

Thus, we have

$$J_m(k_c a) = 0, \tag{B.23}$$

or $k_c a = \alpha_{mn}$ where $\alpha_{mn}$ is $n^{th}$ root of $J_m(x)$. Each of modes has a cutoff frequency ($f_{c_{mn}}$) given by

$$f_{c_{mn}} = \left[\frac{c}{2\pi}\right]\left[\frac{\alpha_{mn}}{a}\right] . \tag{B.24}$$

---

Table B.1: Values of $\alpha_{mn}$ for TM modes of a circular waveguide [40].

| m | $\alpha_{m1}$ | $\alpha_{m2}$ | $\alpha_{m3}$ |
|---|---|---|---|
| 0 | 2.405 | 5.520 | 8.654 |
| 1 | 3.832 | 7.016 | 10.174 |
| 2 | 5.135 | 8.417 | 11.620 |

# APPENDIX C

# MECHANICAL DIAGRAM

## C.1 Drawing Diagram

### C.1.1 Front view reactor chamber

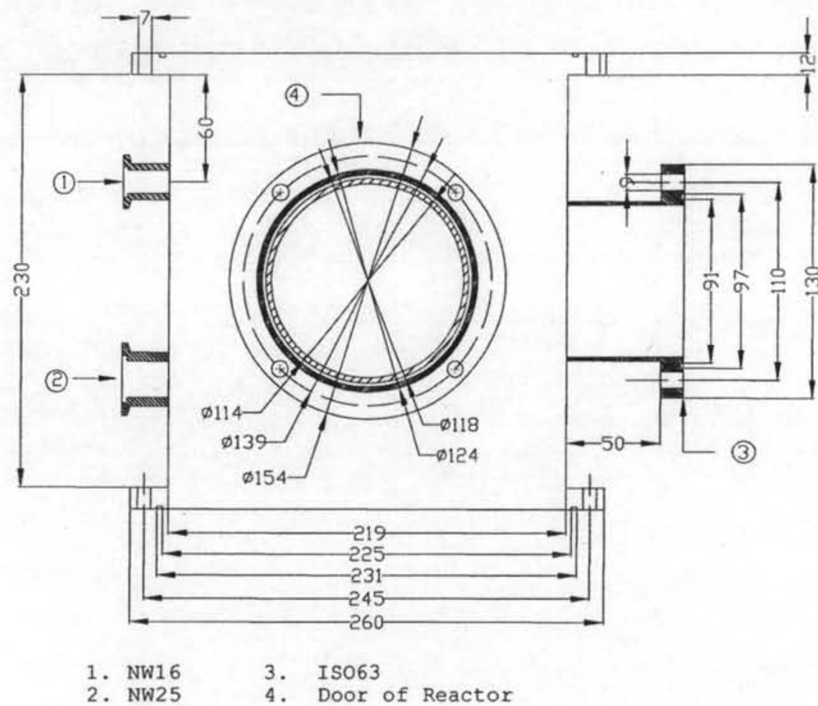


Figure C.1: Vacuum chamber in front view dimension

### C.1.2 Top and bottom plates

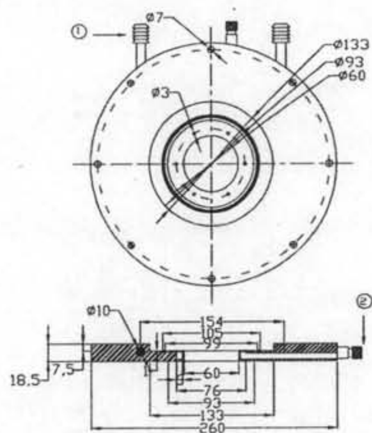


Figure C.2: Donut plate dimension

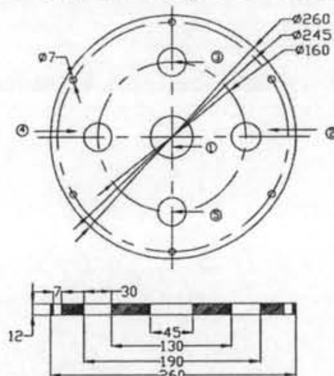


Figure C.3: Bottom plate dimension

# APPENDIX D

# MAGNETRON HEAD

## D.1 Magnetron Head

### D.1.1 Magnetron type: MB2422A-130CF

| Characteristic | Specification | Typical |
|---|---|---|
| Frequency of operation: | 2470 MHz | 2460 MHz |
| Frequency variations: | | +/- 10 MHz |
| CW Power Output: | 1400 W | 1260 W |
| Anode Voltage: | 450 mA | 400 mA |
| Filament Voltage (standby) | 4.8 V | 4.4 V |
| Filament Current: | 15.5 A | 14 A |
| RF launch type: | rectangular or oven cavity | |
| Efficiency: | approx: 70 % | |
| Basis Type: | 2M137 (Panasonic) | |
| Cooling: | | |
| Water-cooled | 3 l/min; 3 bar | |
| Net weight: | approx: 1.5 kg | |

# VITAE

Mr. Nopporn Rujisamphan was born on January 19, 1980 in Bangkok province, Thailand. He has obtained the Bachelor Degree of Science in Physics from Khon Kaen University in 2001.

## Conference Presentations:

### International Presentations

N. Rujisamphan, V. Amornkitbamrung, and B. Paosawatyanyong. LOW COST MICROWAVE PLASMA REACTOR FOR DIAMOND FILM DEPOSITION. *2$^{nd}$ Mathematics and Physical Science Graduate Congress*, National University of Singapore, Singapore (13-14 December 2006): P7

N. Rujisamphan, V. Amornkitbamrung, and B. Paosawatyanyong. Design and Construction of a Thermal-like plasma system. *3$^{rd}$ INTERNATIONAL CONFERENCE ON THE FRONTIERS OF PLASMA PHYSICS AND TECHNOLOGY*, Amari Atrium Hotel, Bangkok (5-9 March 2007)

### Local Presentations

N. Rujisamphan, V. Amornkitbamrung, and B. Paosawatyanyong. DESIGN AND CONSTRUCTION OF MICROWAVE PLASMA REACTOR FOR DIAMOND FILM DEPOSITION. 32$^{th}$ *Congress on Science and Technology of Thailand*, Bangkok, Thailand (10-12 October 2006): D 01100

N. Rujisamphan, V. Amornkitbamrung, and B. Paosawatyanyong. EFFECT OF $CH_4$ CONCENTRATION AND TOTAL PRESSURE ON THE GROWTH OF CARBON COMPOSITE THIN FILM USING MICROWAVE PLASMA DEPOSITION TECHNIQUE. *SIAM PHYSICS CONGRESS 2007*, The rose Garden Riverside, Nakorn Pathom, Thailand (22-24 March 2007): A21